Eight International Conference on Liquid Atomization and Spray Systems, Pasadena, CA, USA, July 2000

Droplet Impact on a Tube: Simulations and Experiments

M. Pasandideh-Fard, M. Bussmann, S. Chandra* and J. Mostaghimi
Department of Mechanical and Industrial Engineering
University of Toronto
Toronto, Canada

Abstract

The impact of a water droplet on a stainless steel tube was studied using both numerical simulations and experiments. A 3D numerical model of Bussmann et al. [1] for free-surface flows (such as an impacting droplet) was extended to include internal obstacles (such as a solid tube) in the fluid computational domain. The results of the model were compared with experimental photographs for the impact of a 2 mm water droplet on two tube sizes: 3.18 mm (0.125 in) and 6.35 mm (0.25 in) O.D.; the impact velocity was 1 m/s and 1.2 m/s on the two tubes, respectively. The droplet impacting on the smaller tube size pinched off the tube surface. On the bigger tube size, however, surface tension effects arrested droplet downward flow on the tube surface; as a result, there was no droplet pinch off in this case. The good qualitative and quantitative agreement between the results of simulations and experimental photographs demonstrated the numerical model to be well suited for simulating free-surface flows over internal obstacles in general, and droplet spraying on tubes in particular.

Introduction

The impact of an individual liquid droplet against a solid surface is an outcome of many spray applications. Most studies, both experimental and numerical, have considered the axisymmetric impact of a droplet against a flat solid surface, which may be considered two-dimensionally. Yet the solid surface geometry is often more complicated. For example, Hardalupas et al. [2] recently presented experimental results of the impact of droplets onto solid spheres of similar curvature, with application to the operation of fluidized beds. And while this is a geometry that can still be considered two-dimensionally, many others cannot. Yao et al. [3] presented results of the impact of water droplets onto the edge of heated thin steel strips, a geometry of interest during the reflooding phase of a nuclear reactor loss-of-coolant accident.

Of interest here is the impact of a droplet onto a cylindrical tube, to demonstrate the efficacy of a numerical technique presented previously [1]. Such a geometry is common in applications such as agricultural and medicinal sprays. Hung and Yao [4] presented experimental results of such a geometry, and characterized the phenomenon according to the relative diameters of the tube and the droplet. In general terms, as tube size increases, fluid adheres more easily to a tube surface, and thus a larger tube tends to be more disruptive of a periodic flow of droplets. The impact and accumulation of fluid is complex, and depends not only on the geometry of impact, but on fluid properties and the wettability of the solid surface.

The numerical method presented here is an extension of a fixed-grid three-dimensional model presented previously [1]. Earlier simulations, of the impact of a droplet onto a flat incline and onto a sharp edge, could be defined along gridlines. Many geometries, like a cylindrical tube, cannot be handled in this way. The model has thus been extended to include the definition of internal obstacles within the grid, to accommodate such geometries. Results are presented of the 1 m/s and 1.2 m/s impacts of a 2 mm diameter water droplet onto tubes of two different diameters, and the results compared with photographs taken of corresponding impacts. The simulation results compare well with experiment, and demonstrate that the methodology is applicable to the simulation of such complex phenomena.

Experimental Method

The experimental method is similar to that previously described by Chandra and Avedisian [5] and by Pasandideh-Fard et al. [6]. Single droplets are formed by slowly pumping distilled water through a hypodermic needle until the droplets detach under their own weight. Droplet diameter is uniformly 2 mm. The droplets fall onto a securely mounted horizontal stainless steel tube (either 3.18 mm (0.125 in) or 6.35 mm (0.25 in) O.D.) polished with 600 grit emery paper.

* Corresponding author

The distance between the needle tip and the point of impact is set to yield the 1 m/s and 1.2 m/s impact velocities. A single 35 mm photograph is taken of any one instant during an impact, as determined by a set time delay between droplet release and the illumination provided by a strobe of 8 μs duration. The photographs of any particular instant from one droplet to the next are sufficiently repeatable that a complete impact sequence may be reconstructed from individual photographs of different droplets.

Numerical Method

Fluid Flow. Fluid flow in an impacting droplet was modeled using a finite difference solution of the Navier-Stokes equations in a 3D Cartesian coordinate system assuming laminar, incompressible flow. The flow Reynolds number (assuming radial flow over a flat plate in the droplet after impact) was estimated to be at most 10^4, too small to induce turbulence. The surface profile of the deforming droplet was defined using the ''fractional volume of fluid'' scheme. In this method, a scalar function f is defined as the fraction of a cell volume occupied by fluid. f is assumed to be unity when a cell is fully occupied by the fluid and zero for an empty cell. Cells with values of $0<f<1$ contain a free surface. Surface tension is modeled as a volume force acting on fluid near the free surface. Details of the fluid flow model are given by Bussmann et al. [1,7].

Internal Obstacle. The tube in the computational domain is an internal obstacle which affects the fluid flow. We treat the internal obstacles as a special case of two-phase flow, in which the first phase is the fluid, with volume fraction Θ, and the second phase is the obstacle, with volume fraction (1-Θ). The obstacle is characterized as a fluid of infinite density and zero velocity. The volume fraction Θ is a scalar field whose value is equal to one in the fluid and zero in the obstacle. With this definition, Θ is a perfect step function only when obstacle boundaries coincide with lines of the computational mesh. In general, however, obstacle boundaries arbitrarily snake through the mesh, cutting through cells. This gives rise to Θ values in the range $0\leq\Theta\leq1$, which is necessary to avoid a 'stair-step' model of a curved interior obstacle boundary. Those cells having a value of Θ satisfying $0<\Theta<1$ are termed "partial flow cells" because a portion Θ of their finite difference volume is open to flow and the remaining portion (1-Θ) is occupied by an obstacle closed to flow. In the presence of internal obstacles, the finite difference equations are modified by defining a volume fraction Θ at the cell center, and area fractions Θ_x , Θ_y and Θ_z at the cell faces in the x, y and z directions, respectively. Based on this method, the final modified continuity, momentum and VOF equations are [8,9]

$$\vec{\nabla}\cdot(\Theta\vec{V})=0 \tag{1}$$

$$\frac{\partial(\Theta\vec{V})}{\partial t}+(\Theta\vec{V}\cdot\vec{\nabla})\vec{V}=\frac{-\Theta}{\rho}p+\Theta\upsilon\nabla^2\vec{V}+\frac{\Theta}{\rho}\vec{F_b} \tag{2}$$

$$\frac{\partial f}{\partial t}+(\Theta\vec{V}\cdot\vec{\nabla})f=0 \tag{3}$$

where $\vec{V}$ represents the velocity vector, p the pressure, ρ the density, υ the kinematic viscosity and $\vec{F_b}$ any body forces acting on the fluid.

Boundary Conditions for the Obstacle. Boundary conditions which must be imposed on the surface of the obstacle are velocity boundary conditions and contact angle conditions at the contact line (the line at which the solid, liquid and gas phases meet). Discretization of boundary conditions is done as follows. No-slip conditions are applied by defining "fictitious" velocities within obstacle cells adjacent to fluid cells. These conditions are only set for obstacle cells with a zero value of Θ. Velocities at the faces of these obstacle cells are set such that normal and tangential velocities at the liquid-obstacle interface become zero (no-slip condition).

Contact angles must be properly set at all points on the fluid contact line on the obstacle surface. The contact angle here is defined as the angle between the unit normal vector $\hat{n}$ directed into the liquid phase and the unit normal $\hat{n}_w$ directed into the obstacle at every point of the contact line. To evaluate $\hat{n}$ we use the values of the volume fraction f according to the following equation

$$\hat{n}=\frac{\vec{\nabla}f}{\left|\vec{\nabla}f\right|} \tag{4}$$

Detailed finite difference approximation of Eq. 4 is given by Bussmann et al. [1]. For this scheme to work when including obstacles we need to assign pseudo volume fractions to obstacle cells adjacent to the liquid. The approach used was to mirror values of f from fluid cells into adjacent obstacle cells. Evaluation of $\hat{n}_w$ is done similarly

$$\hat{n}_w=\frac{\vec{\nabla}(1-\Theta)}{\left|\vec{\nabla}(1-\Theta)\right|} \tag{5}$$

The unit normals $\hat{n}$ and $\hat{n}_w$ are evaluated at any vertex of the obstacle cells adjacent to the contact line. The angle between the two unit normals at every point on the contact line can be obtained from

$$\cos(\alpha)=\hat{n}\cdot\hat{n}_w \tag{6}$$

Since the fluid-obstacle interface is a spatial surface, the direction of unit normals $\hat{n}$ and $\hat{n}_w$ varies with

location on the contact line. As a result, the angle α is a spatial angle that varies at every point on the contact line. Proper setting of contact angles at the contact line requires that the unit normal $\hat{n}$ at every point of the contact line is redirected such that the angle between $\hat{n}$ and $\hat{n}_w$ is set to the dynamic contact angle θ_d instead of the angle α. If $\hat{n}_r$ is the redirected unit normal into the liquid phase we will have

$$\hat{n}_r = \frac{\sin(\theta_d)}{\sin(\alpha)}\hat{n} + \frac{\sin(\alpha - \theta_d)}{\sin(\alpha)}\hat{n}_w \qquad (7)$$

Finally, the evaluation of $\hat{n}_r$ from the above equation requires a known value of the dynamic contact angle at every point of the contact line. A simple model, introduced by Bussmann el al. [1], is used to evaluate contact angle as a function of contact line velocity. The model requires values of only two contact angles, at a rapidly advancing and a rapidly receding contact line. For the cases under consideration in this study, water droplets on tubes, we used the values suggested by Bussmann el al. [1] for the impact of a water droplet on an incline: 110° and 40° at the advancing and receding contact lines, respectively.

The modified Navier-Stokes equations were solved on an Eulerian, rectangular, staggered mesh in a 3D Cartesian coordinate system. The droplet was discretized with a grid spacing equal to 1/15 of the droplet radius. Numerical computations were performed on a Sun Ultra Enterprise 450 workstation. A typical CPU time was three days.

Results

We present the results for the impact of a 2 mm water droplet with a velocity of 1 m/s and 1.2 m/s on two different tube sizes, 3.18 mm and 6.35 mm O.D., respectively. The point of impact of the droplet was offset from the tube center in both cases when viewed along the axis of the tube.

Figure 1 shows images, generated by the numerical model, and corresponding photographs of successive stages of droplet impact on a tube with an outside diameter of 3.18 mm. The impact velocity was 1 m/s. Times shown were measured from the moment of impact. The droplet impacted the tube on one side, the center of the droplet offset 1.55 mm from the center of the tube along the direction normal to the impact (Fig. 1 at 0.0 ms). Right after the impact, the droplet spread on the surface of the tube and moved down on the side of the impact as shown after 0.4 ms in Fig. 1. The downward fluid motion on this side continued to the end of the process. The droplet spreading on the other side of the tube, however, stopped after 0.4 ms. As the droplet was moving down it spread and recoiled along the tube axis as shown in a video animation of the numerical results viewed from an angle [10]. Close inspection of the numerical results [10] showed that the droplet spread to its maximum extent along the tube axis until 2.5 ms after the impact. After this time, the droplet was recoiling along the tube axis; the recoil is seen in Fig. 1 after 4.6 ms in both simulations and photographs. As a result of the downward flow, after 4 ms, the bulk of the droplet was not in contact with the tube surface. This resulted in a column of liquid being suspended from the tube. The tip of this column began to neck off, forming a droplet that detached 11.0 ms after initial impact. A second smaller droplet also formed from the fluid tail at the bottom of the tube; this droplet pinched off at 12 ms from the impact (see Fig. 1). The model captured the formation and detachment of both droplets at the exact times as observed experimentally (see Fig. 1). The rest of the fluid tail withdrew to the bottom surface of the tube. The remaining fluid on the tube moved slowly to the bottom of the tube as shown from both numerical results and photographs. The good qualitative and quantitative agreement between the simulation results and experimental photographs demonstrated that the numerical model is well suited for simulating free-surface flows with internal obstacles in general, and droplet spraying on tubes in particular.

The results of the simulation model and experimental photographs for the second case, droplet impact on a 6.35 mm tube size, are shown in Fig. 2. The impact velocity in this case was 1.2 m/s. Similar to the previous case, the droplet impacted the tube with an offset of 1.85 mm from the center of the tube along the direction normal to the impact (Fig. 2 in 0.0 ms). The droplet was moving down on the side of the impact as soon as 0.4 ms from the impact. The droplet spreading in the other side of the tube, however, stopped after 0.8 ms from the impact. Compared to the previous case, there was more fluid contact with the tube surface (because of a bigger size tube). More kinetic energy was, therefore, lost due to the viscous dissipation. As a result, downward fluid motion was arrested by surface tension forces within 6 ms after impact. Compared to the impact on the smaller tube, although the impact velocity was higher in this case, there was no droplet pinch off. A video animation of the numerical results viewed from an angle [11] showed the maximum spread along the tube axis after 3 ms from the impact. The droplet recoiled after this time; the droplet recoil is seen in Fig. 2 in images corresponding to 6 ms and 8 ms after impact. A good qualitative agreement between the results of simulation and experiments was found in this case. The simulation model, however, predicted less downward fluid movement as seen in Fig. 2. Surface tension and interfacial forces become dominant towards the end of droplet spread, and eventually arrest

the downward flow of the droplet. It is likely that errors in our estimate of the dynamic liquid-solid contact angle, which varies with both time and location around the droplet periphery, are responsible for the observed discrepancies between the simulations and experiments.

Conclusions

A 3D computational model of free-surface flows including internal obstacles was developed. The model was an extension of the Bussmann et al. model [1]. The model was used to simulate the impact of a water droplet on a stainless steel tube. The results of the model were compared with experimental photographs for the impact of a 2 mm water droplet on two tube sizes: 3.18 mm and 6.35 mm O.D.; the impact velocity was 1 m/s and 1.2 m/s on the two tubes, respectively. The droplet impacting on the smaller tube size pinched off the tube surface. On the bigger tube size, however, surface tension effects arrested droplet downward flow on the tube surface; as a result, there was no droplet pinch off in this case. The good qualitative and quantitative agreement between the results of simulations and experimental photographs demonstrated the numerical model to be well suited for simulating free-surface flows over internal obstacles in general, and droplet spraying on tubes in particular.

References

1. Bussmann M., Mostaghimi J. and Chandra S., *Phys. Fluids* 11: 1406-1417 (1999).
2. Hardalupas Y., Taylor AMKP and Wilkins J. H., *Proceedings of ILASS-Europe'98*, 122-127 (1998).
3. Yao S. C., Hochreiter L. E. and Cai K. Y., *J. of Heat Transfer* 110: 214-220 (1988).
4. Hung L. S. and Yao S. C., *Int. J. of Multiphase Flow* 25: 1545-1559 (1999).
5. Chandra S. and Avedisian C. T., *Proc. R. Soc. London A*, 432: 13-41 (1991).
6. Pasandideh-Fard M., Qiao Y. M., Chandra S. and Mostaghimi J., *Phys. Fluids* 8: 650-659 (1996).
7. Bussmann M., *Ph.D. Thesis*, University of Toronto, (2000).
8. Pasandideh-Fard M., Bhola R., Chandra S. and Mostaghimi J., *Int. J. of Heat Mass Transfer* 41: 2929-2945 (1998).
9. Pasandideh-Fard M., *Ph.D. Thesis*, University, (1998).
10. Video animation of simulation results (viewed from an angle) for the impact of a 2 mm water droplet on a 3.18 mm (0.125 in) O.D. tube, to be presented with this paper.
11. Video animation of simulation results (viewed from an angle) for the impact of a 2 mm water droplet on a 6.35 mm (0.25 in) O.D. tube, to be presented with this paper.

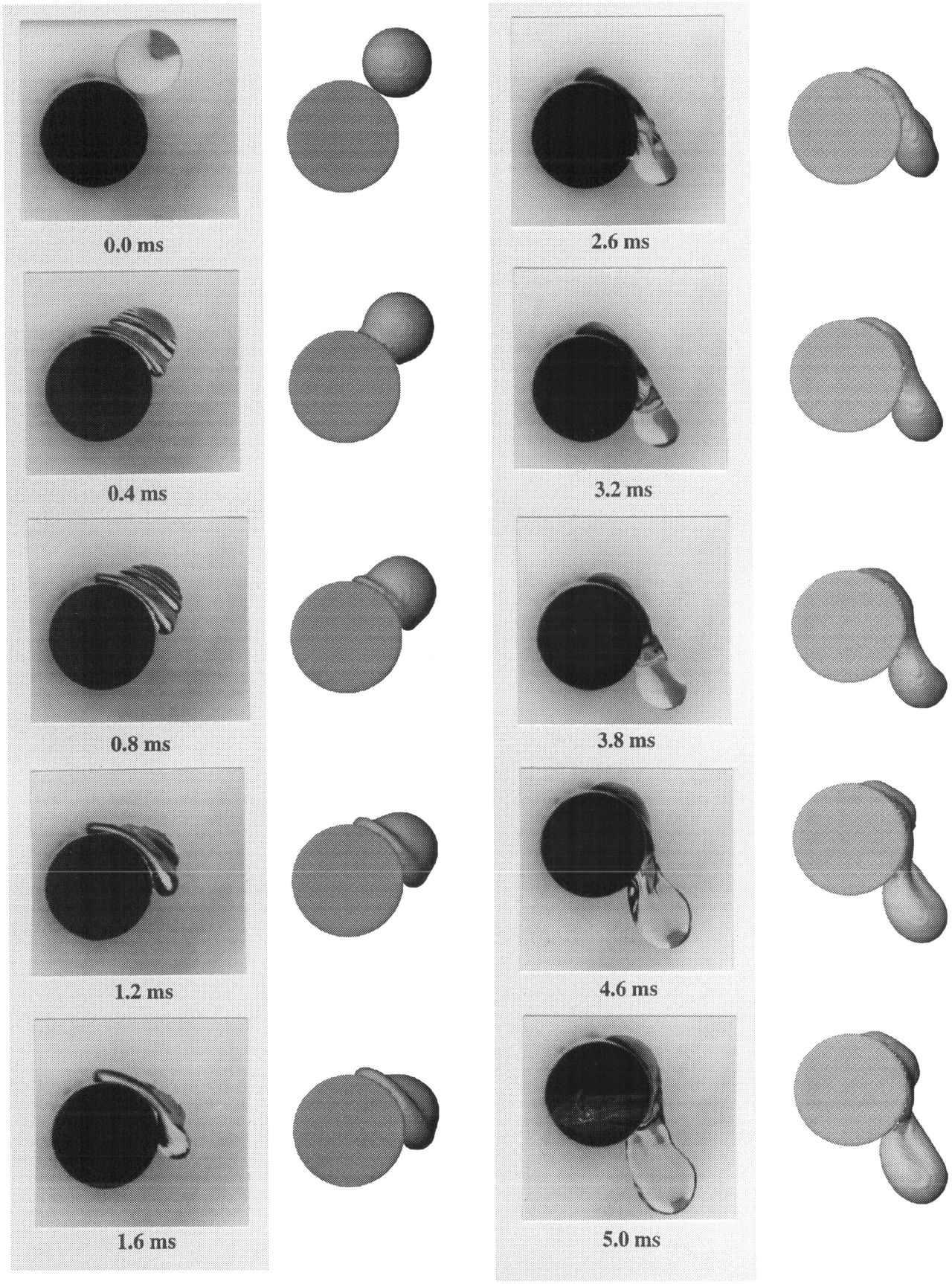

Figure 1. Side-view images of the impact of a 2 mm dia water droplet at 1 m/s onto a stainless steel tube with an outside dia of 3.18 mm (0.125 in); the droplet center offset 1.55 mm from the tube center. Photographs at left, corresponding simulation results at right. Times measured from the moment of impact.

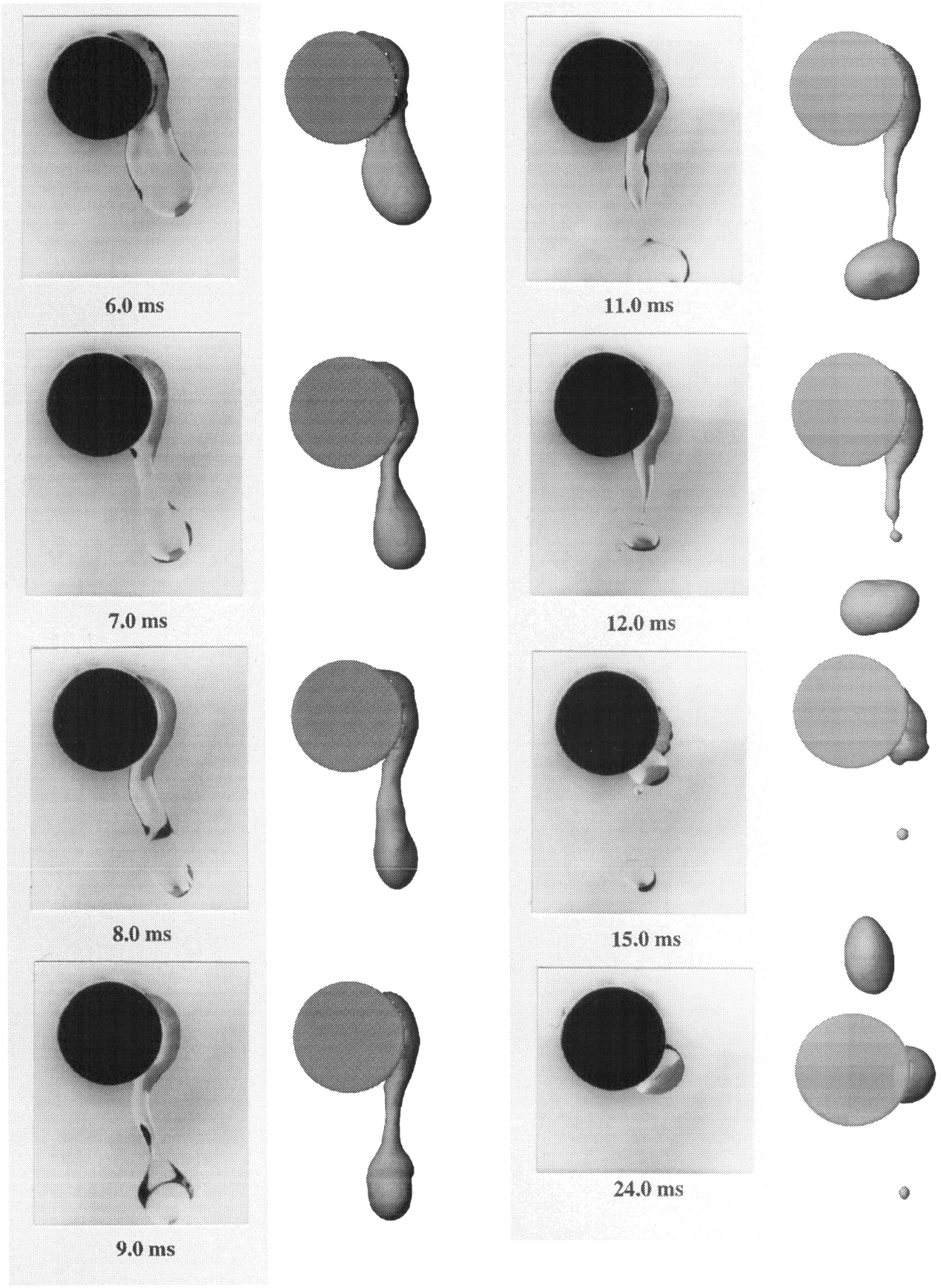

Figure 1. Continued.

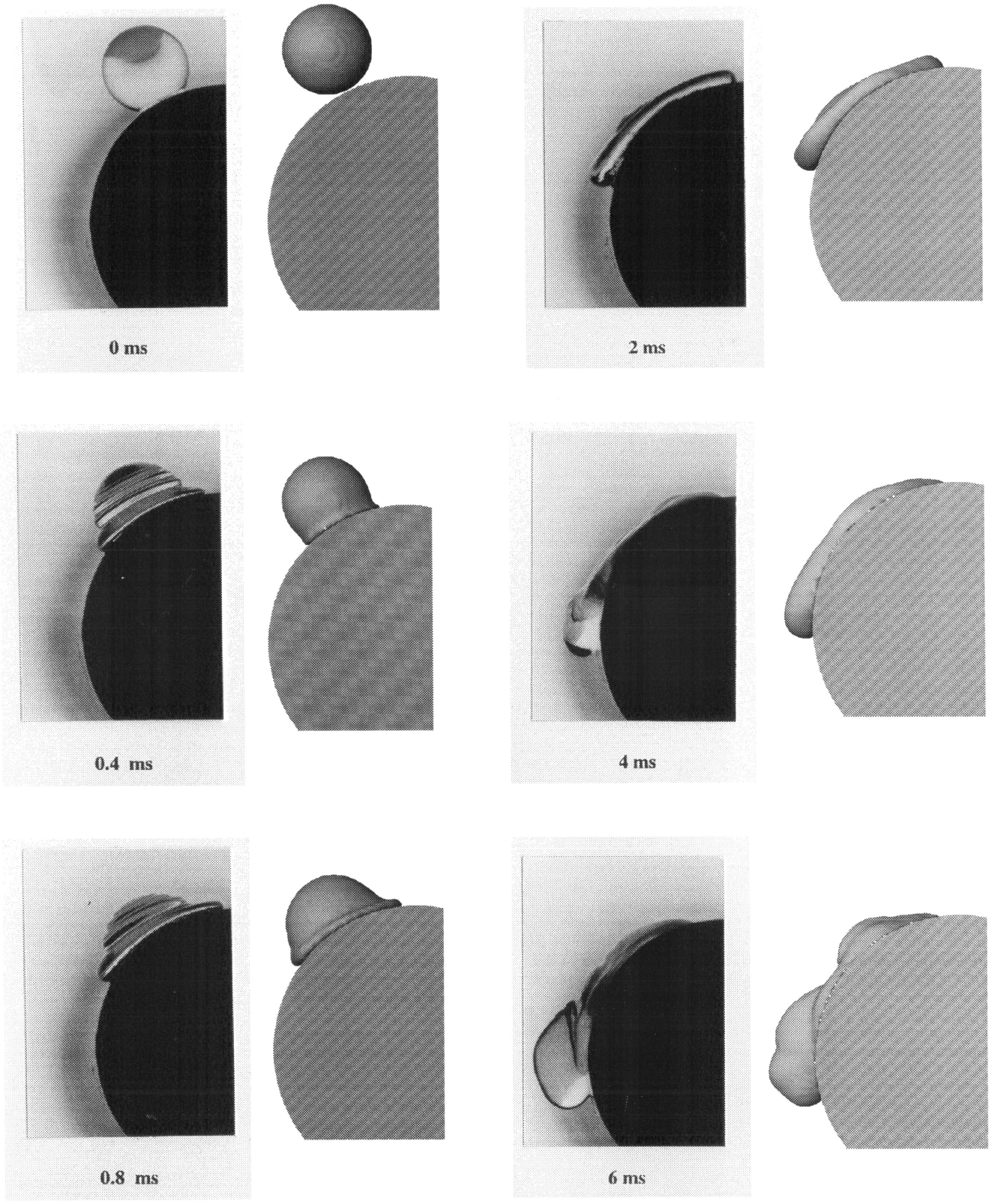

Figure 2. Side-view images of the impact of a 2 mm dia water droplet at 1.2 m/s onto a stainless steel tube with an outside dia of 6.35 mm (0.25 in); the droplet center offset 1.85 mm from the tube center. Photographs at left, corresponding simulation results at right. Times measured from the moment of impact.

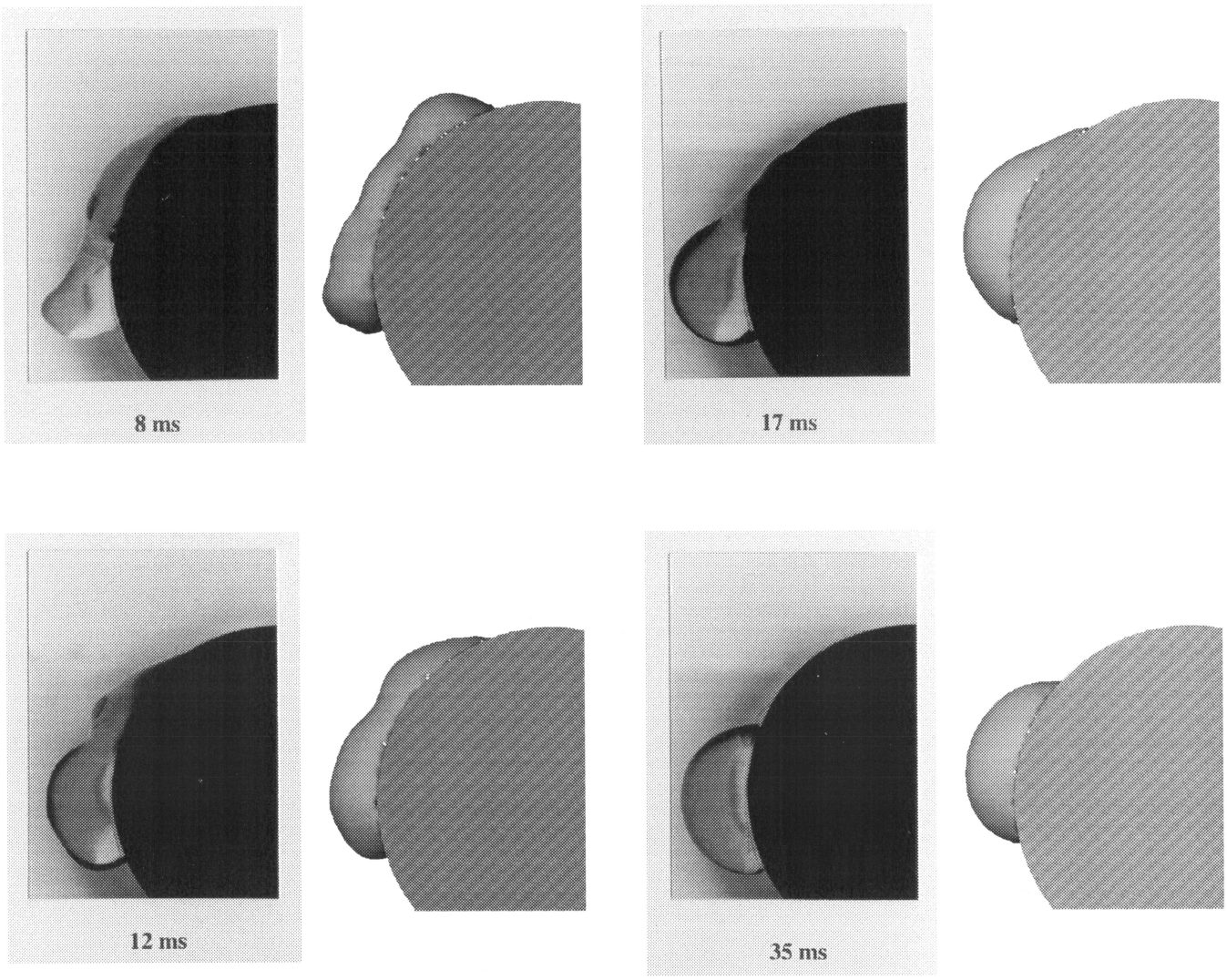

Figure 2. Continued.